Band alignment at GaN/single-layer WSe_2 interface

Malleswararao Tangi[1], Pawan Mishra[1], Chien-Chih Tseng[2], Tien Khee Ng[1], Mohamed Nejib Hedhili[3], Dalaver H. Anjum[3], Mohd Sharizal Alias[1], Nini Wei[3], Lain-Jong Li[2], and Boon S. Ooi[1*]

[1]Photonics Laboratory, Computer, Electrical, and Mathematical Sciences and Engineering (CEMSE) Division, King Abdullah University of Science and Technology (KAUST), Thuwal 23955-6900, Saudi Arabia.

[2]Physical Science and Engineering (PSE) Division, King Abdullah University of Science and Technology (KAUST), Thuwal 23955-6900, Saudi Arabia.

[3]Imaging and Characterization Laboratory, King Abdullah University of Science and Technology (KAUST), Thuwal 23955-6900, Saudi Arabia.

ABSTRACT: We study the band discontinuity at the GaN/single-layer (SL) WSe_2 heterointerface. The GaN thin layer is epitaxially grown by molecular beam epitaxy on chemically vapor deposited SL-WSe_2/c-sapphire. We confirm that the WSe_2 was formed as an SL from structural and optical analyses using atomic force microscopy, scanning transmission electron microscopy, micro-Raman, absorbance, and micro-photoluminescence spectra. The determination of band offset parameters at the GaN/SL-WSe_2 heterojunction is obtained by high-resolution x-ray photoelectron spectroscopy, electron affinities and the electronic bandgap values of SL-WSe_2 and GaN. The valence band and conduction band offset values are determined to be 2.25±0.15 and 0.80±0.15 eV respectively, with type II band alignment. The band alignment parameters determined here provide a route towards the integration of group III nitride semiconducting materials with transition metal dichalcogenides (TMDs) for designing and modeling of their heterojunction based electronic and optoelectronic devices.

KEYWORDS: GaN, single layer WSe_2, 3D/2D heterojunction, HRXPS, band alignment, molecular beam epitaxy

*Corresponding author electronic mail: boon.ooi@kaust.edu.sa

1. INTRODUCTION

Group-III nitrides, GaN as a primary material, are well demonstrated with enormous applications in high efficiency electronic and optoelectronics devices such as high electron mobility transistors, light emitting diodes, and laser diodes.[1–4] Recently, group VI transition metal dichalcogenides (TMDs) in the form of MX_2 has emerged as a novel atomic layered material system with challenging thermoelectric, electronic and optoelectronic properties.[5–8] Among the TMDs, tungsten diselenide (WSe_2) in a single layer form is of potential interest for such devices owing to its direct bandgap of ≈1.65 eV and prominent transport properties.[9,10] GaN has small lattice mismatch of ≈3.2%, ≈1.0% and ≈0.8% with majorly studied TMDs such as WSe_2, tungsten disulfide (WS_2) and molybdenum disulfide (MoS_2)[11], respectively, in comparison to commonly used substrates such as sapphire, SiC and Si.[12,13] Moreover, recent advances in the integration of 2D-layered materials with wide band gap group III nitride semiconductors is exciting due to their variety of applications in high current tunnel diodes.[14,15] Several efforts were made to grow GaN on closely lattice matched TMDs. Yamada *et al.* presented the growth of GaN on bulk MoS_2 by plasma-enhanced molecular beam epitaxy[16]. There were recent attempts to grow GaN on large area MoS_2 and WS_2 layers,[11,17] layered MoS_2 on GaN epilayers[18] by chemical vapor deposition (CVD) growth techniques and layer transferred p-MoS_2 on GaN[14]. Though the deposition of large area single-layer WSe_2 on sapphire exhibiting direct bandgap has been demonstrated,[9,19] the growth of GaN on such large area monolayered WSe_2 has not yet been explored.

So far, the band offset parameters were determined for either group III nitrides on various other semiconducting materials or solely TMDs based dissimilar heterostructures using X-ray photoemission spectroscopic core-levels evaluated with respect to the valence band maximum and bandgap studies. Though, the band offset parameters (junction type: valence band offset- ΔE_v & conduction band offset- ΔE_c) are measured for various heterojunctions in the literature.[20–25] Recently we have reported the growth of GaN on SL-MoS_2 and the band alignment parameters (Type-II: 1.86±0.08 & 0.56±0.10 eV) for GaN/SL-MoS_2 hetero-interface.[26] The band offset parameters (valence band offset (VBO)-ΔE_v and conduction band offset (CBO)-ΔE_c) and type of junction by HRXPS for epitaxially formed GaN/SL-WSe_2 hetero-interface is yet to be experimentally investigated. The determination of band offset parameters is required to study the group III nitride/TMDs heterojunction based devices. These hybrid heterojunctions, exhibiting type I and II band alignments, can be utilized as TMD quantum well based light emitting devices

and the tunnel diodes, respectively.[6,15] Thus, the growth of GaN/SL-WSe_2 and the determination of band offsets are necessary to provide a route towards the integration of group III nitrides with TMDs for designing the electronic and optoelectronic devices.

In this report, in order to study the band discontinuity at the GaN/SL-WSe_2 heterointerface, thin GaN layers were epitaxially grown on a CVD prepared SL-WSe_2. The sustainability of SL-WSe_2 during GaN growth is confirmed by the atomic force microscopy (AFM), micro-photoluminescence (μPL) and Raman spectroscopies. In addition, the band offset parameters for GaN/SL-WSe_2 heterojunction were determined using high-resolution x-ray photoelectron spectroscopy (HRXPS) and electronic band gap values of respective constituent layers in the heterojunction.

2. EXPERIMENTAL SECTION

The growth experiments of GaN on WSe_2/c-sapphire substrates were carried out by Veeco 930 Gen plasma assisted molecular beam epitaxy (PAMBE) system at substrate temperature of 500 $^{\circ}$C. The large area WSe_2 SLs were prepared on c-sapphire substrates using CVD and the details can be found elsewhere[19]. The ion and a cryo pumps were employed to attain a base pressure of 3×10^{-11} Torr and oxygen partial pressure $<10^{-11}$ Torr, as obtained by a residual gas analyzer (RGA). The substrates were thermally outgassed in introduction chamber at 200 $^{\circ}$C for 30 mins, further cleaning was carried out in preparation chamber at 300 $^{\circ}$C for 60 mins and in the growth chamber at 400 $^{\circ}$C for 30 mins. For GaN growth, the nitrogen plasma source was operated with the flow rate of 1 standard cubic centimeter per minute (sccm) and RF power of 300 W and Ga metal was evaporated by standard Knudsen cell with beam equivalent pressure (BEP) value of 2.10×10^{-8} Torr. Prior to this, thin AlN buffer layer was grown. The corresponding chamber pressure was $\approx2.5\times10^{-5}$ Torr. The thickness of the GaN epilayer (sample C) is measured to be ≈500 nm. The thickness of GaN layer in sample B was estimated to be 6±1 nm from growth rate calibrations. The Agilent technologies 5400 atomic force microscopy was used in tapping mode to acquire the surface morphology of the samples. Structural quality of GaN epilayer was investigated by CuK_{α} High Resolution X-ray Diffraction (HRXRD) having four-bounce Ge(022) monochromator. High-angle annular dark field scanning transmission electron microscopy (HAADF-STEM) was utilized by operating a probe-corrected FEI Titan at an acceleration voltage of 300 kV. A cross- sectional TEM specimen of sample B was prepared by using FEI's Helios Dual Beam focused ion beam

(FIB)/SEM equipped with an Omniprobe. Electron energy loss spectroscopy (EELS) acquisition was performed by using Gatan's GIF Quantum of Model 966. Using Horiba Aramis room temperature (RT) μPL, the emission of GaN and WSe_2 layers was deduced with excitation lines of He-Cd laser of 325 nm and He-Ne laser of 633 nm, respectively. Absorbance spectra were acquired with a Shimadzu UV3600 spectrophotometer equipped with integrating sphere. The high-resolution XPS measurements were carried out using a Kratos Axis Ultra DLD spectrometer equipped with a monochromatic Al K_α X-ray source ($h\nu$ = 1486.6 eV) operating at 150 W, a multi-channel plate and delay line detector under a vacuum of ~10^{-9} mbar. The high-resolution spectra were collected within the limits of spatial resolution at a fixed analyzer pass energy of 20 eV. In order to eliminate the shifts in the HRXPS spectra associated with the surface charging effect, the measurements were acquired both with and without electron beam charge compensation. For both cases, no changes were observed in the determined band alignment. In absence of electron beam charge, the surface of samples was electrically connected with a clean copper (Cu) foil. The remnant binding energy shifts were referenced to the adventitious carbon (C 1s) signal.[27–29] In this study, CVD grown SL-WSe_2 (sample A), MBE grown GaN on SL-WSe_2 (sample B) and GaN epilayer (sample C) were used to determine the band offsets at GaN/SL-WSe_2 hetero-interface.

3. RESULTS AND DISCUSSION

To investigate the surface morphology, root mean square (rms) roughness of GaN/WSe2 (B) and GaN epilayer (C), and thickness of WSe_2 layer (A), AFM scans were carried out in tapping mode. Figures 1(a-c) show the AFM surface topography scans collected on samples C, A and B, respectively. The AFM images were obtained at different scales to view the fine features according to surface smoothness of the formed films. Color bars on top of the respective images in Figure 1 show height contrast of the features. From Figure 1(a), the root mean square (rms) surface roughness for GaN film is ≈2 nm. Moreover, AFM is one of the most commonly used technique to determine the number of monolayers of TMDs samples. The thickness of the large area WSe_2 layer is found to be ≈0.76 nm from the line profile as shown in Figure 1(b) for sample A, which is in agreement with the thickness of Se-W-Se single-layer.[19] The inset to Figure 1(b) displays the optical microscopy image of large area WSe_2 layer. Figure 1(c) shows the AFM surface morphology for sample B exhibiting surface rms roughness of ≈4 nm which is higher than that of relaxed GaN epilayer (sample C) that results from the lattice mismatch between thin GaN and

WSe_2. Thus, AFM study confirms that the CVD deposited large area WSe_2 is in the form of a single layer. Further, HRXRD measurements were performed to investigate the crystalline structure and quality of the GaN epilayer (sample C). Figure 1(d) presents the 2θ-ω scans, which were obtained on the symmetric (on-axis) and asymmetric (off-axis) planes of sample C. Asymmetric planes were studied in skew symmetric geometry.[4] Figure 1(d) displays c-oriented peaks: at GaN(0002) at 34.52°, GaN(0004) at 73.20° along with the buffer layer AlN(0002) at 35.89° and Al_2O_3 substrate (0006) at 41.45°, respectively. The asymmetric reflection shows GaN($10\bar{1}1$) peak at 36.81° GaN($20\bar{2}2$) at 78.77° along with the buffer layer peak AlN($10\bar{1}1$) at 38.50° and substrate peak Al_2O_3($11\bar{2}3$) at 43.08°, respectively. The respective inset shows the ω scans for on-axis GaN(0002) and off-axis GaN($10\bar{1}1$) reflections, with broadening values of ≈350 and ≈980 arc-sec, respectively. Thus, from HRXRD analysis, sample C possess single crystalline wurtzite structure grown along c-axis exhibiting moderate crystal quality.

HAADF-STEM studies were performed on sample B (GaN/WSe_2/c-sapphire) to confirm the existence and the thickness of GaN and WSe_2 layers. Figure 2(a) shows the cross sectional HAADF-STEM image recorded on sample B which is prepared by FIB. Prior to this, the Ti metal layer having thickness of ≈500 nm was deposited on sample B by e-beam evaporation method to avoid any physical damage of thin GaN and WSe_2 layers at the heterojunction caused by focused ion beams while the sample preparation was done for STEM studies. This reveals that the thickness of GaN/WSe_2 heterojunction is ≈7 nm. Figure 2(b) shows the magnified STEM image of Figure 2(a) obtained across the GaN/WSe_2/c-sapphire heterojunction (sample B). STEM-EELS imaging data sets were acquired to generate the elemental maps of W, Se, Ga and Al elements by employing W-M (1809 eV), Se-L (1436 eV), Ga-L (1117 eV), and Al-K (1560 eV) EELS edges, respectively. The elements W, Se, Ga and Al across the junction are, respectively, represented by Blue, Green, Red, and Yellow colored pixels. Figure 2(c) depicts the elemental mapping of heterojunction showing the existence of both W and Se atoms at the interface. A STEM-EDS line profile was generated to re-confirm the presence of SL-WSe2 that is sandwiched between sapphire substrate and GaN thin film. Figure 2(d) represents the EDS line profiles obtained for elements Al, Ga, W and Se across the junction. The intensity of line profiles for W and Se atoms increases in the region of SL-WSe_2 whereas the line profiles for Ga and Al elements exhibit high intensity in the regions of overgrown GaN and underlying sapphire substrates, respectively, as shown in Figure 2(d). Therefore, it is

noted that the line profiles in Figure 2(d) were in accordance with the respective elemental color mapping as depicted in Figure 2(c). Thus, Figures 2 (b-d) depict the existence of WSe_2 in the form of single layer having thickness of ≈0.78 nm which is in corroboration with AFM analysis. Overall, the HAADF-STEM analysis is a clear evidence of the formation of GaN/SL-WSe_2 heterojunction.

Micro-Raman spectroscopy was used to investigate the optical quality as well as to ensure that the CVD grown WSe_2 is an SL. Figure 3(a-d) shows the Raman spectra for WSe_2/c-sapphire, GaN/WSe_2/c-sapphire and GaN/c-sapphire. In order to obtain the enhanced Raman signal from GaN and WSe_2 layers, the measurements were carried out with excitation lines of 325 and 633 nm by which signal can overcome the reduced resonant excitation effect.[26,30] Thus, both the excitation sources are required to collect the high intensity phonon modes from the individual layer in GaN/SL-WSe_2 heterojunction as described in Figure 3(b and c). The two characteristic peaks in Figure 3(a and b) observed at 248 cm^{-1} and 259 cm^{-1} are attributed to E^1_{2g} and A_{1g} phonon modes.[10,19].These modes correspond to the in plane vibration of W and Se atoms (E^1_{2g}) and out of plane vibration of Se atoms (A_{1g}) in WSe_2. The intensity ratio (I_A/I_E) of these modes is higher than the reported values which can be attributed to the variation in doping levels.[31] The observed peaks at 222, 241, 377 and 398 cm^{-1} stem from the WSe_2 layer which are consistent with the previous studies.[10,32] The peaks represented by asterisks are from the sapphire substrate. The absence of a peak at ≈307 cm^{-1} confirms that the formed WSe_2 is a single layer which is corroborated by AFM studies. These results also show the sustainability of WSe_2 layer during the growth of GaN in PAMBE. In consequence of the reduced resonant excitation effect[26], in Figure 3(b), E^H_2 mode of GaN exhibits lower intensity than the E^1_{2g} and A_{1g} phonon modes of WSe_2 while the sample B is excited with 633 nm line. In contrast, in Figure 3(c), the intensity of E^H_2 mode for GaN is higher than that of the phonon modes (E^1_{2g} and A_{1g}) of WSe_2 with 325 nm excitation. Further, Figure 3(c) shows a low intensity single peak for both E^1_{2g} and A_{1g} phonon modes which is in good agreement with the literature.[33–35] In Figure 3(b and c), the E^H_2 peak of thin GaN grown on WSe_2 is significantly blue shifted from that of the bulk GaN (sample C) having the peak at 568.5±0.5 cm^{-1} which results from the strain accompanied by the pseudomorphic growth of GaN on SL-WSe_2/c-sapphire. Thus, AFM, STEM and micro-Raman measurements confirm that the existence of SL-WSe_2 during the growth of GaN.

In order to investigate the optical quality of both WSe_2, bulk like GaN epilayer and GaN/WSe_2 (samples A-C) room temperature μPL and absorbance measurements were performed. Figure 4 (a and b) show the RT μPL and optical absorbance spectra acquired on GaN epilayer and WSe_2. The optical band edge emissions (E_{opt}^{GaN} and $E_{opt}^{SL-WSe_2}$) for GaN and WSe_2 are observed at ≈3.43 and ≈1.63 eV, respectively. The low intensity PL for sample B could be due to the presence of octahedral phase of WSe_2, which will be discussed later. The WSe_2 (A) and GaN/WSe_2 (B) exhibits the direct optical bandgap which is matching with the value of single layer[23]. As represented in Figure 4(b) the observed states X_A, X_B , $X_{A'}$ and $X_{B'}$ for sample A at ≈1.63, ≈2.08, ≈2.44 and ≈2.91 eV in the absorbance spectrum are the exciton resonances corresponding to the transitions from broken inversion symmetry induced two spin-split valence sub-bands to the conduction band and vice versa[36–38]. Thus, the spin splitting of WSe_2 is observed to be ≈0.45 eV which is smaller than that of $MoSe_2$ exhibiting the largest value of ≈0.55 eV among MX_2 family[39,40]. Hence, this observation confirms that the CVD grown WSe_2 sample is in the form of SL, as corroborated by earlier AFM, STEM and micro-Raman measurements. However, these are not an exact band to band transitions due to the involvement of excitons. The electronic band gap is measure of actual gap of a material which is the summation of optical bandgap and exciton (electron-hole) binding energy ($E_g=E_{opt}+E_b$).[40] Hence, these observed optical bandgap values differ from reported electronic bandgap values of $E_g^{SL-WSe_2}$ =2.08 eV and E_g^{GaN} =3.45 eV by their respective exciton binding energy (E_b) values of ≈0.450 and ≈0.023 eV as reported in the literature.[23,41,42]

High-resolution XPS measurements were extensively used to measure the valence band offset (VBO) of a heterointerface. In order to evaluate VBO at GaN/SL-WSe_2 interface, the energy difference between the Ga and W core levels from the GaN/SL- WSe_2 heterojunction sample and the energy of core levels relative to the respective valence band maximum (VBM) of the GaN epilayer and SL- WSe_2 samples need to be acquired. As the escape depth of photo emitted electrons in HRXPS is significantly low, over grown GaN layer of heterojunction sample has to be thin enough so that the electrons removed from both thin overgrown GaN and underlying SL- WSe_2 layers can be easily examined.[43] However, the surface area of SL-WSe_2 is large enough to carry out the XPS measurements, due to the non-continuity of the WSe_2 film on sapphire substrate, the region of interest on WSe_2/sapphire and GaN/WSe_2 samples was selectively chosen within the

spatial resolution of HRXPS measurements.[23,44] This is executed by comparing the intensity of Ga 2p, W 4f and Al 2p core-levels which allowed us to collect the photoemission signal from solely SL-WSe_2/sapphire and GaN/SL- WSe_2 heterostructures for samples A and B, respectively. Since LMM auger line of Ga at ≈397 eV N overlaps with N 1s core level for Al K_α anode as x-ray source in HRXPS measurements, the N 1s core levels are not considered for the analysis of VBO determination. Furthermore, Ga 3d is also excluded from the analysis as it exists close to the valence band states.[45] Thus, in order to determine the VBO, the core levels W 4f, Se 3d and Ga 2p were used for the analysis. The valence band offset (VBO) for GaN/SL-WSe_2 heterojunction, can be calculated by the method provided by Kraut et al.[46], expressed as

$$\Delta E_v = \left(E^{WSe_2}_{W\,4f_{7/2}} - E^{WSe_2}_{VBM}\right) + \left(E^{GaN/WSe_2}_{Ga\,2p_{3/2}} - E^{GaN/WSe_2}_{W\,4f_{7/2}}\right) - \left(E^{GaN}_{Ga\,2p_{3/2}} - E^{GaN}_{VBM}\right) \quad (1)$$

From Figure 5a (i and ii), the first term of equation (1) deduced by taking into account the position of W $4f_{7/2}$ core-level referenced with respect to the VBM, which is measured to be 31.56±0.10 eV. The values of the valence band maxima (VBM) are determined by extrapolating the linear fit to the leading edge of the valence band to the base level.[47,48] Prior to this, W 4f core-level is deconvoluted so as to access the accurate value that contributed solely from W-Se bonding in SL-WSe_2. In this peak deconvolution process, we use Voigt (mixed Lorentzian-Gaussian) line shapes for fitting the W-Se (trigonal prismatic -2H) and W-O chemical states, respectively, centered at 32.52±0.10 and 36.15±0.10 eV. The later state with low intensity results from WO_3 precursor or excess W metal bonding with the oxygen of c-Al_2O_3 at the interface of WSe_2/c-sapphire during high temperature CVD growth.

In order to evaluate the subsequent term, GaN/SL-WSe_2 sample is used for XPS measurements where we consider the difference between Ga $2p_{3/2}$ and W $4f_{7/2}$ core-levels. Figure 5b (i and ii) depicts the Ga 2p and W 4f core-levels which are acquired on GaN/SL-WSe_2 heterointerface. Figure 5(b-i) represents the Ga 2p core-level which is deconvoluted with Ga-N bonding and any other states are not observed. The Figure 5(b-ii) shows the fitting of W 4f core-level equipped with three W $4f_{7/2}$ chemical states at 30.81±0.10, 31.94±0.10 and 36.17±0.10 eV, ascribed to the W-Se bonding in 1T-WSe_2 (octahedral), W-Se bonding in 2H-WSe_2 (trigonal prismatic), and W-O bonding in WO_3, respectively.[49] The W $4f_{5/2}$ core-level has similar deconvolutions at higher binding energy values differed by ≈2.16 eV from W $4f_{7/2}$ bonding states. The octahedral phase could be due to unintentional N-plasma intercalation of WSe_2 single layer during GaN growth which is as similar as lithium intercalation reported for the case of MoS_2[37]. The presence of

octahedral phase results in the low intensity PL signal for sample B as presented in Figure 4(b). The W-Se bonding peak infers that the sustainability of SL-WSe_2 at GaN growth temperature under UHV oxygen free environment. The absence of any other chemical state associated with W or Se in Ga 2p core-level spectrum is a clear evidence of Vander Waal epitaxy. Thus, the energy difference between W $4f_{7/2}$ and Ga $2p_{3/2}$ core-levels is observed to be 1085.92±0.10 eV as described in Figure 5(b).

The last term indicates the core-level energy 1115.23±0.10 eV of Ga $2p_{3/2}$ measured relative to the respective VBM of 2.27±0.15 eV as shown in Figure 5(c). This VBM measured with respect to the Fermi level for nearly intrinsic GaN which was utilized in the present study is lower than that of the n-type GaN in the literature (2.7 eV).[47] In Figure 5c(i), Ga $2p_{3/2}$ and $2p_{1/2}$ core-levels are deconvoluted with Ga-N bonding state at 1117.50±0.10 and 1144.40±0.10 eV, respectively. The Fermi level position with respect to the VBM as shown in Figure 5(a-ii and c-ii) infers that GaN epilayer and SL-WSe_2 are nearly intrinsic materials. Thus, the VBO from equation (1) is determined to be ≈2.25±0.15 eV. The VBO is also confirmed by using VB spectrum, Se 3d and Ga 2p core levels of samples A and B (see supporting information).

As a result, the substitution of VBO (ΔE_v) obtained from HRXPS analysis (Figure 5) and electronic bandgap (E_g) values of SL-WSe_2 and GaN epilayer in equation (2), allows to measure the conduction band offset (CBO) ΔE_c for GaN/SL-WSe_2 heterostructure.

$$\Delta E_c = E_g^{WSe_2} + \Delta E_v - E_g^{GaN} \qquad (2)$$

Thus, the CBO (ΔE_c) is determined to be 0.88±0.10 eV. Furthermore, the measured CBO value is verified by the Anderson's affinity rule which is defined as the difference between electron affinity values of constituent semiconductors of heterojuction.[50] The electron affinity (the energy separation between vacuum level and CBM) values χ^{GaN}, χ^{SL-WSe_2} of GaN and SL-WSe_2 were ≈4.1 and ≈3.3 eV, respectively.[51,52] UPS measurements were performed to measure the electron affinity of GaN. Here, electron affinity (χ) of SL-WSe_2 is extracted using the formula $\chi = \phi - (E_g - E_F)$ from our earlier reported work function value deduced by ultraviolet photoelectron spectroscopic (UPS) measuremetns[52], where ϕ is the work function (3.61 eV) and E_g is the electronic bandgap (2.08 eV) and E_F is the Fermi level position with respect to VBM (1.8 eV) of an SL-WSe_2. For more details see the supporting information. It should be noted that

electron affinity is material specific and independent of the Fermi level position. Hence, from Anderson's rule, calculated CBO for GaN/SL-WSe_2 heterojunction is 0.8 eV. The determined CBO value of 0.88±0.15 eV from HRXPS studies in the present study is consistent with the value (0.8 eV) obtained by affinity rule, which facilitates in understanding the electron transport properties across the heterojunction.

Thereby, the experimentally measured offset parameters from this study are presented as a schematic of band discontinuity diagram in Figure 6 which pertains to type-II heterostructure.

4. CONCLUSIONS

In conclusion, GaN epitaxial thin layers were deposited on SL-WSe_2/c-sapphire substrates by PAMBE to study the band discontinuity at GaN/SL-WSe_2 heterointerface. We confirm that the CVD deposited WSe_2 is a single-layer by complementary characterization tools such as AFM, HAADF-STEM, micro-Raman modes, absorbance and μPL studies. The determination of band offset parameters at GaN/SL-WSe_2 heterostructure was carried out by utilizing the HRXPS, electron affinities and electronic band gap values. We determine the valence band and conduction band offset values, respectively, of 2.25±0.15 eV and 0.8±0.15 eV with type II band alignment at GaN/SL-WSe_2 heterostructure. This demonstration of unprecedented band offset parameters renders a route towards the integration of 3D group III nitride materials with 2D transition metal dichalcogenide layers.

ASSOCIATED CONTENT

Supporting Information: Confirmation of valence band offset by using Ga 2p and Se 3d HRXPS core levels. Determination of electron affinity for GaN and SL-WSe_2 by ultraviolet photoelectron spectroscopy (UPS).

AUTHOR INFORMATION

Corresponding author:

*Email: boon.ooi@kaust.edu.sa

Notes The authors declare no competing financial interest.

ACKNOWLEDGEMENTS

We acknowledge the financial support from King Abdulaziz City for Science and Technology (KACST), Grant No. KACST TIC R2-FP-008 and baseline funding BAS/1/1614-01-01 of the King Abdullah University of Science and Technology (KAUST).

REFERENCES

(1) Nakamura, S.; Senoh, M.; Nagahama, S.; Iwasa, N.; Yamada, T.; Matsushita, T.; Kiyoku, H.; Sugimoto, Y.; Kozaki, T.; Umemoto, H.; Sano, M.; Chocho, K. Violet InGaN/GaN/AlGaN-Based Laser Diodes with an Output Power of 420 mW. *Jpn. J. Appl. Phys.* **1998**, *37* (Part 2, No. 6A), L627–L629.

(2) Shen, L.; Heikman, S.; Moran, B.; Coffie, R.; Zhang, N.-Q.; Buttari, D.; Smorchkova, I. P.; Keller, S.; DenBaars, S. P.; Mishra, U. K. AlGaN/AlN/GaN High-Power Microwave HEMT. *IEEE Electron Device Lett.* **2001**, *22* (10), 457–459.

(3) Zhao, C.; Ng, T. K.; Elafandy, R. T.; Prabaswara, A.; Consiglio, G. B.; Ajia, I. A.; Roqan, I. S.; Janjua, B.; Shen, C.; Eid, J.; Alyamani, A. Y.; El-Desouki, M. M.; Ooi, B. S. Droop-Free, Reliable, and High-Power InGaN/GaN Nanowire Light-Emitting Diodes for Monolithic Metal-Optoelectronics. *Nano Lett.* **2016**, *16* (7), 4616–4623.

(4) Tangi, M.; De, A.; Ghatak, J.; Shivaprasad, S. M. Electron Mobility of Self-Assembled and Dislocation Free InN Nanorods Grown on GaN Nano Wall Network Template. *J. Appl. Phys.* **2016**, *119* (May), 205701.

(5) Radisavljevic, B.; Radenovic, A.; Brivio, J.; Giacometti, V.; Kis, A. Single-Layer MoS2 Transistors. *Nat. Nanotechnol.* **2011**, *6* (3), 147–150.

(6) Baugher, B. W. H.; Churchill, H. O. H.; Yang, Y.; Jarillo-Herrero, P. Optoelectronic Devices Based on Electrically Tunable P-N Diodes in a Monolayer Dichalcogenide. *Nat. Nanotechnol.* **2014**, *9* (4), 262.

(7) Pu, J.; Kanahashi, K.; Cuong, N. T.; Chen, C.-H.; Li, L.-J.; Okada, S.; Ohta, H.; Takenobu, T. Enhanced Thermoelectric Power in Two-Dimensional Transition Metal Dichalcogenide Monolayers. *Phys. Rev. B* **2016**, *94* (1), 14312.

(8) Li, M.-Y.; Shi, Y.; Cheng, C.-C.; Lu, L.-S.; Lin, Y.-C.; Tang, H.-L.; Tsai, M.-L.; Chu, C.-W.; Wei, K.-H.; He, J.-H.; Chang, W.-H.; Suenaga, K.; Li, L.-J. Epitaxial Growth of a Monolayer WSe_2-MoS_2 Lateral P-N Junction with an Atomically Sharp Interface. *Science*

(80-.). **2015**, *349* (6247), 524.

(9) Eichfeld, S. M.; Hossain, L.; Lin, Y.; Piasecki, A. F.; Kupp, B.; Birdwell, A. G.; Burke, R. A.; Lu, N.; Peng, X.; Li, J.; Azcatl, A.; McDonnell, S.; Wallace, R. M.; Kim, M. J.; Mayer, T. S.; Redwing, J. M.; Robinson, J. A. Highly Scalable, Atomically Thin WSe_2 Grown via Metal-Organic Chemical Vapor Deposition. *ACS Nano* **2015**, *9* (2), 2080–2087.

(10) Huo, N.; Tongay, S.; Guo, W.; Li, R.; Fan, C.; Lu, F.; Yang, J.; Li, B.; Li, Y.; Wei, Z. Novel Optical and Electrical Transport Properties in Atomically Thin WSe_2/MoS_2 P-N Heterostructures. *Adv. Electron. Mater.* **2015**, *1* (5), 1400066.

(11) Gupta, P.; Rahman, A. A.; Subramanian, S.; Gupta, S.; Thamizhavel, A.; Orlova, T.; Rouvimov, S.; Vishwanath, S.; Protasenko, V.; Laskar, M. R.; Xing, H. G.; Jena, D.; Bhattacharya, A. Layered Transition Metal Dichalcogenides: Promising near-Lattice-Matched Substrates for GaN Growth. *Sci. Rep.* **2016**, *6* (March), 23708.

(12) Reshchikov, M. A.; Morkoç, H. Luminescence Properties of Defects in GaN. *J. Appl. Phys.* **2005**, *97* (2005), 61301.

(13) Liu, L.; Edgar, J. H. Substrates for Gallium Nitride Epitaxy. *Mater. Sci. Eng. R Reports* **2002**, *37* (3), 61–127.

(14) II, E. W. L.; Lee, C. H.; Paul, P. K.; Ma, L.; McCulloch, W. D.; Krishnamoorthy, S.; Wu, Y.; Arehart, A. R.; Rajan, S. Layer-Transferred MoS_2/GaN PN Diodes. *Appl. Phys. Lett.* **2015**, *107* (10), 103505.

(15) Krishnamoorthy, S.; Lee, E. W.; Lee, C. H.; Zhang, Y.; McCulloch, W. D.; Johnson, J. M.; Hwang, J.; Wu, Y.; Rajan, S. High Current Density 2D/3D Esaki Tunnel Diodes. *Appl. Phys. Lett.* **2016**, *183505* (June), 183505.

(16) Yamada, A.; Ho, K. P.; Maruyama, T.; Akimoto, K. Molecular Beam Epitaxy of GaN on a Substrate of MoS_2 Layered Compound. *Appl. Phys. A Mater. Sci. Process.* **1999**, *69* (1), 89–92.

(17) Mishra, P.; Tangi, M.; Ng, T. K.; Hedhili, M. N.; Anjum, D. H.; Alias, M. S.; Tseng, C.-C.; Li, L.-J.; Ooi, B. S. Impact of N-Plasma and Ga-Irradiation on MoS_2 Layer in Molecular Beam Epitaxy. *Appl. Phys. Lett.* **2017**, *110* (1), 12101.

(18) Ruzmetov, D.; Zhang, K.; Stan, G.; Kalanyan, B.; Bhimanapati, G. R.; Eichfeld, S. M.; Burke, R. A.; Shah, P. B.; O'Regan, T. P.; Crowne, F. J.; Birdwell, A. G.; Robinson, J. A.; Davydov, A. V; Ivanov, T. G. Vertical 2D/3D Semiconductor Heterostructures Based on

Epitaxial Molybdenum Disulfide and Gallium Nitride. *ACS Nano* **2016**, *10*, 3580–3588.

(19) Huang, J. K.; Pu, J.; Hsu, C. L.; Chiu, M. H.; Juang, Z. Y.; Chang, Y. H.; Chang, W. H.; Iwasa, Y.; Takenobu, T.; Li, L. J. Large-Area Synthesis of Highly Crystalline WSe_2 Monolayers and Device Applications. *ACS Nano* **2014**, *8* (1), 923–930.

(20) King, P. D. C.; Veal, T. D.; Kendrick, C.; Bailey, L.; Durbin, S.; McConville, C. F. InN/GaN Valence Band Offset: High-Resolution X-Ray Photoemission Spectroscopy Measurements. *Phys. Rev. B* **2008**, *78* (3), 33308.

(21) Martin, G.; Strite, S.; Botchkarev, A.; Agarwal, A.; Rockett, A.; Morkoç, H.; Lambrecht, W. R. L.; Segall, B. Valence-Band Discontinuity between GaN and AlN Measured by X-Ray Photoemission Spectroscopy. *Appl. Phys. Lett.* **1994**, *65* (5), 610–612.

(22) Bhat, T. N.; Kumar, M.; Rajpalke, M. K.; Roul, B.; Krupanidhi, S. B.; Sinha, N. Band Alignment Studies in InN/p-Si(100) Heterojunctions by X-Ray Photoelectron Spectroscopy. *J. Appl. Phys.* **2011**, *109* (12), 123707.

(23) Chiu, M.-H.; Zhang, C.; Shiu, H.-W.; Chuu, C.-P.; Chen, C.-H.; Chang, C.-Y. S.; Chen, C.-H.; Chou, M.-Y.; Shih, C.-K.; Li, L.-J. Determination of Band Alignment in the Single-Layer MoS_2/WSe_2 Heterojunction. *Nat. Commun.* **2015**, *6* (May), 7666.

(24) Siol, S.; Hellmann, J. C.; Tilley, S. D.; Graetzel, M.; Morasch, J.; Deuermeier, J.; Jaegermann, W.; Klein, A. Band Alignment Engineering at Cu_2O/ZnO Heterointerfaces. *ACS Appl. Mater. Interfaces* **2016**, *8* (33), 21824–21831.

(25) Qiao, L.; Li, W.; Xiao, H.; Meyer, H. M.; Liang, X.; Nguyen, N. V.; Weber, W. J.; Biegalski, M. D. Electronic Structure and Band Alignment at an Epitaxial Spinel/perovskite Heterojunction. *ACS Appl. Mater. Interfaces* **2014**, *6* (16), 14338–14344.

(26) Tangi, M.; Mishra, P.; Ng, T. K.; Hedhili, M. N.; Janjua, B.; Alias, M. S.; Anjum, D. H.; Tseng, C. C.; Shi, Y.; Joyce, H. J.; Li, L. J.; Ooi, B. S. Determination of Band Offsets at GaN/single-Layer MoS_2 Heterojunction. *Appl. Phys. Lett.* **2016**, *109* (3), 32104.

(27) Bersch, E.; Rangan, S.; Bartynski, R. A.; Garfunkel, E.; Vescovo, E. Band Offsets of Ultrathin High- K Oxide Films with Si. *Phys. Rev. B* **2008**, *78*, 85114.

(28) King, S. W.; Paquette, M. M.; Otto, J. W.; Caruso, A. N.; Brockman, J.; Bielefeld, J.; Kuhn, M.; French, B.; King, S. W.; Paquette, M. M.; Otto, J. W.; Caruso, A. N.; Brockman, J.; Bielefeld, J.; French, M.; Kuhn, M.; French, B. Valence and Conduction Band Offsets at Amorphous Hexagonal Boron Nitride Interfaces with Silicon Network Dielectrics. *Appl.*

Phys. Lett. **2014**, *104*, 102901.

(29) Distefano, J.; Lin, Y.; Robinson, J.; Glavin, N. R.; Voevodin, A. A.; Brockman, J.; Kuhn, M.; French, B.; King, S. W. Band Alignment at Molybdenum Disulphide / Boron Nitride / Aluminum Oxide Interfaces. *J. Electron. Mater.* **2016**, *45* (2), 983–988.

(30) Tangi, M.; Mishra, P.; Janjua, B.; Ng, T. K.; Anjum, D. H.; Prabaswara, A.; Yang, Y.; Albadri, A. M.; Alyamani, A. Y.; El-Desouki, M. M.; Ooi, B. S. Bandgap Measurements and the Peculiar Splitting of E2H Phonon Modes of $In_xAl_{1-x}N$ Nanowires Grown by Plasma Assisted Molecular Beam Epitaxy. *J. Appl. Phys.* **2016**, *120* (4), 45701.

(31) Chakraborty, B.; Bera, A.; Muthu, D. V. S.; Bhowmick, S.; Waghmare, U. V.; Sood, A. K. Symmetry-Dependent Phonon Renormalization in Monolayer MoS_2 Transistor. *Phys. Rev. B* **2012**, *85* (16), 161403(R).

(32) Huang, J.; Yang, L.; Liu, D.; Chen, J.; Fu, Q.; Xiong, Y.; Lin, F.; Xiang, B. Large-Area Synthesis of Monolayer WSe_2 on a SiO_2/Si Substrate and Its Device Applications. *Nanoscale* **2015**, *7* (9), 4193–4198.

(33) Zeng, H.; Liu, G.-B.; Dai, J.; Yan, Y.; Zhu, B.; He, R.; Xie, L.; Xu, S.; Chen, X.; Yao, W.; Cui, X. Optical Signature of Symmetry Variations and Spin-Valley Coupling in Atomically Thin Tungsten Dichalcogenides. *Sci. Rep.* **2013**, *3* (4), 1608.

(34) Sugawara, K.; Sato, T.; Tanaka, Y.; Souma, S.; Takahashi, T. Spin- and Valley-Coupled Electronic States in Monolayer WSe_2 on Bilayer Graphene. *Appl. Phys. Lett.* **2015**, *107* (7), 71601.

(35) del Corro, E.; Botello-Méndez, A.; Gillet, Y.; Elias, A. L.; Terrones, H.; Feng, S.; Fantini, C.; Rhodes, D.; Pradhan, N.; Balicas, L.; Gonze, X.; Charlier, J.-C.; Terrones, M.; Pimenta, M. A. Atypical Exciton–Phonon Interactions in WS_2 and WSe_2 Monolayers Revealed by Resonance Raman Spectroscopy. *Nano Lett.* **2016**, *16*, 2363.

(36) Mak, K. F.; Shan, J. Photonics and Optoelectronics of 2D Semiconductor Transition Metal Dichalcogenides. *Nat. Photonics* **2016**, *10* (4), 216–226.

(37) Eda, G.; Yamaguchi, H.; Voiry, D.; Fujita, T.; Chen, M.; Chhowalla, M. Photoluminescence from Chemically Exfoliated MoS_2. *Nano Lett.* **2011**, *11* (12), 5111–5116.

(38) Jin, W.; Yeh, P. C.; Zaki, N.; Zhang, D.; Sadowski, J. T.; Al-Mahboob, A.; Van Der Zande, A. M.; Chenet, D. A.; Dadap, J. I.; Herman, I. P.; Sutter, P.; Hone, J.; Osgood, R. M. Direct Measurement of the Thickness-Dependent Electronic Band Structure of MoS_2 Using Angle-

Resolved Photoemission Spectroscopy. *Phys. Rev. Lett.* **2013**, *111* (10), 106801.

(39) Zhu, Z. Y.; Cheng, Y. C.; Schwingenschlögl, U. Giant Spin-Orbit-Induced Spin Splitting in Two-Dimensional Transition-Metal Dichalcogenide Semiconductors. *Phys. Rev. B* **2011**, *84* (15), 153402.

(40) Ugeda, M. M.; Bradley, A. J.; Shi, S.-F.; da Jornada, F. H.; Zhang, Y.; Qiu, D. Y.; Ruan, W.; Mo, S.-K.; Hussain, Z.; Shen, Z.-X.; Wang, F.; Louie, S. G.; Crommie, M. F. Giant Bandgap Renormalization and Excitonic Effects in a Monolayer Transition Metal Dichalcogenide Semiconductor. *Nat. Mater.* **2014**, *13* (12), 1091–1095.

(41) Zhou, S. Q.; Wu, M. F.; Hou, L. N.; Yao, S. D.; Ma, H. J.; Nie, R.; Tong, Y. Z.; Yang, Z. J.; Yu, T. J.; Zhang, G. Y. An Approach to Determine the Chemical Composition in InGaN/GaN Multiple Quantum Wells. *J. Cryst. Growth* **2004**, *263* (1–4), 35–39.

(42) Muth, J. F.; Lee, J. H.; Shmagin, I. K.; Kolbas, R. M.; Casey, H. C.; Keller, B. P.; Mishra, U. K.; DenBaars, S. P. Absorption Coefficient, Energy Gap, Exciton Binding Energy, and Recombination Lifetime of GaN Obtained from Transmission Measurements. *Appl. Phys. Lett.* **1997**, *71* (18), 2572.

(43) Fadley, C. S. Atomic-Level Characterization of Materials with Core- and Valence-Level Photoemission: Basic Phenomena and Future Directions. *Surf. Interface Anal.* **2008**, *40* (13), 1579–1605.

(44) Choi, J.; Zhang, H.; Choi, J. H. Modulating Optoelectronic Properties of Two-Dimensional Transition Metal Dichalcogenide Semiconductors by Photoinduced Charge Transfer. *ACS Nano* **2016**, *10*, 1671–1680.

(45) Zanatta, A. R.; Hammer, P.; Alvarez, F. Photoelectron Spectroscopic Study of Amorphous GaAsN Films. *Appl. Phys. Lett.* **2000**, *76* (16), 2211.

(46) Kraut, E. A.; Grant, R. W.; Waldrop, J. R.; Kowalczyk, S. P. Precise Determination of the Valence-Band Edge in X-Ray Photoemission Spectra: Application to Measurement of Semiconductor Interface Potentials. *Phys. Rev. Lett.* **1980**, *44* (24), 1620–1623.

(47) King, S. W.; Ronning, C.; Davis, R. F.; Benjamin, M. C.; Nemanich, R. J. Dependence of (0001) GaN/AlN Valence Band Discontinuity on Growth Temperature and Surface Reconstruction. *J. Appl. Phys.* **1998**, *84* (4), 2086–2090.

(48) Tangi, M.; Kuyyalil, J.; Shivaprasad, S. M. Optical Bandgap and near Surface Band Bending in Degenerate InN Films Grown by Molecular Beam Epitaxy. *J. Appl. Phys.* **2013**,

114 (15), 153501.

(49) Ambrosi, A.; Sofer, Z.; Pumera, M. 2H → 1T Phase Transition and Hydrogen Evolution Activity of MoS_2, $MoSe_2$, WS_2 and WSe_2 Strongly Depends on the MX_2 Composition. *Chem. Commun.* **2015**, *51* (40), 8450.

(50) Anderson, R. L. Germanium-Gallium Arsenide Heterojunctions [Letter to the Editor]. *IBM J. Res. Dev.* **1960**, *4* (3), 283–287.

(51) Bougrov, V.; Levinshtein, M. E.; Rumyantsev, S. L.; Zubrilov, A. *Properties of Advanced Semiconductor Materials :* GaN, AlN, InN, BN, SiC, SiGe; Levinshtein, M. E., Rumyantsev, S. L., Shur, M. S., Eds.; John Wiley & Sons, Inc.: New York, 2001.

(52) Chen, C.-H.; Wu, C.-L.; Pu, J.; Chiu, M.-H.; Kumar, P.; Takenobu, T.; Li, L.-J. Hole Mobility Enhancement and P -Doping in Monolayer WSe_2 by Gold Decoration. *2D Mater.* **2014**, *1* (3), 34001.

Figures and captions.

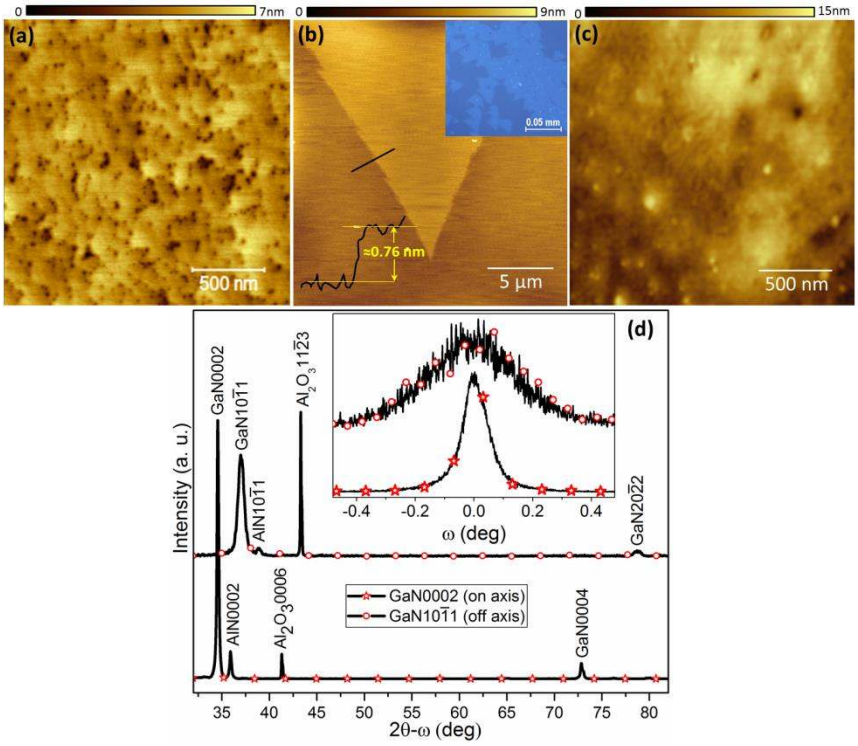

Figure 1 shows the AFM scans for (a) GaN epilayer, (b) WSe_2 and (c) GaN/WSe_2 samples, respectively. The line profile of 1(b) represents the thickness of WSe_2 layer. The inset to Figure 1(b) is optical microscopy image of WSe_2 sample. Figure 1(d) shows the HRXRD 2θ-ω scans of on-axis and off-axis reflections and the inset shows the respective ω-scans acquired on GaN epilayer.

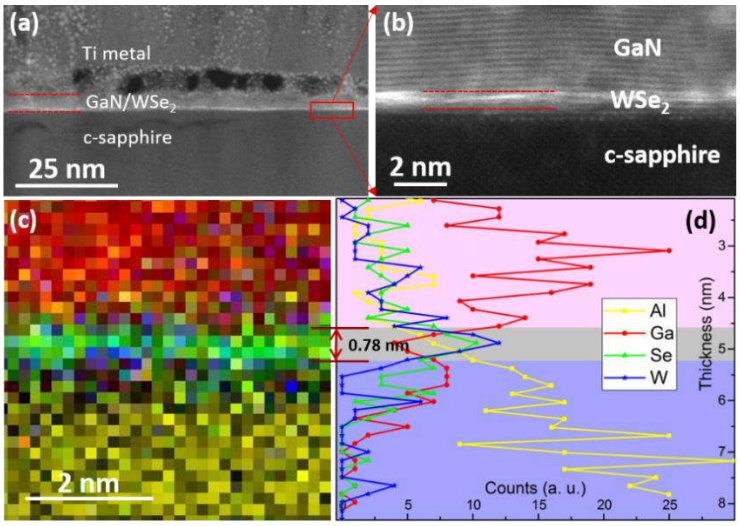

Figure 2 (a and b) show the low and high magnification cross-sectional images of high-angle annular dark field - scanning transmission electron microscopy (HAADF-STEM) for sample B. (c) shows the STEM-EELS elemental color maps (W-Blue, Se-Green, Ga-Red, and Al-Yellow). Figure 2(d) represents the STEM-EDS elemental line profiles acquired across the GaN/WSe_2/c-sapphire heterojunction.

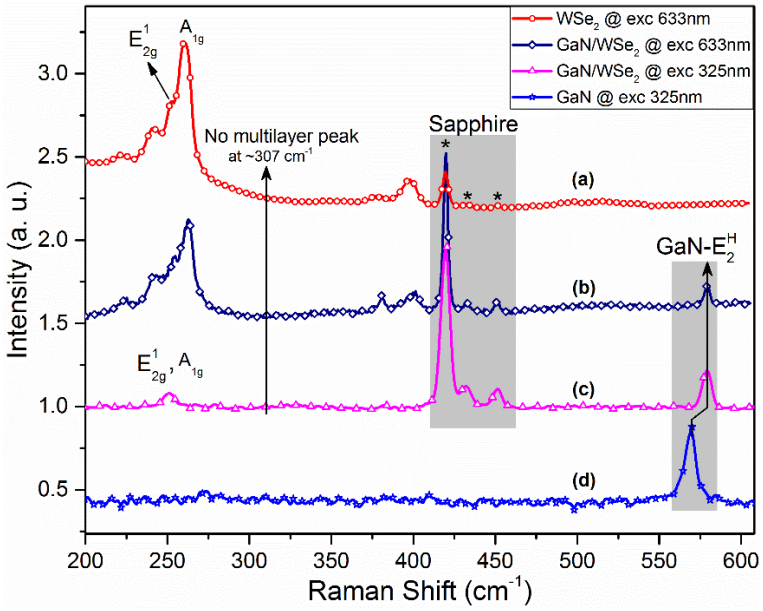

Figure 3(a-d) show the micro-Raman spectra of samples A-C collected on WSe_2, GaN/WSe_2 and bulk like GaN samples, respectively. Here, He-Cd (325 nm) and He-Ne (633 nm) excitation sources ($E_{exc} > E_g$) were used to enhance the Raman signal based on the band gap of each material.

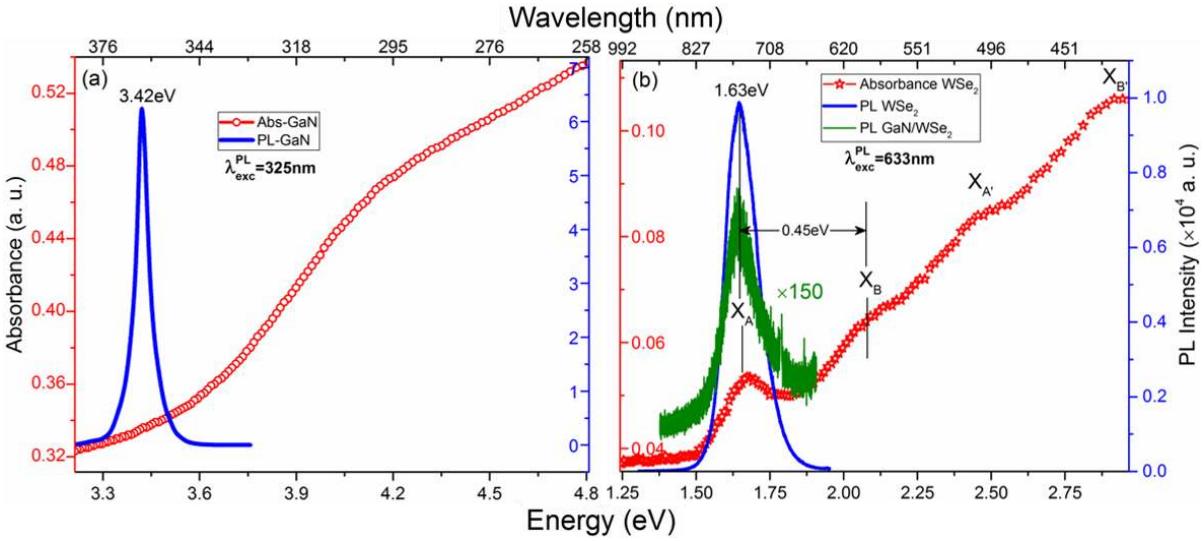

Figure 4(a and b) show the micro-photoluminescence (right y-axis) and absorbance spectra (left y-axis) of GaN and WSe_2 samples. The green colored PL peak in Figure 4(b) is for GaN/WSe_2 sample.

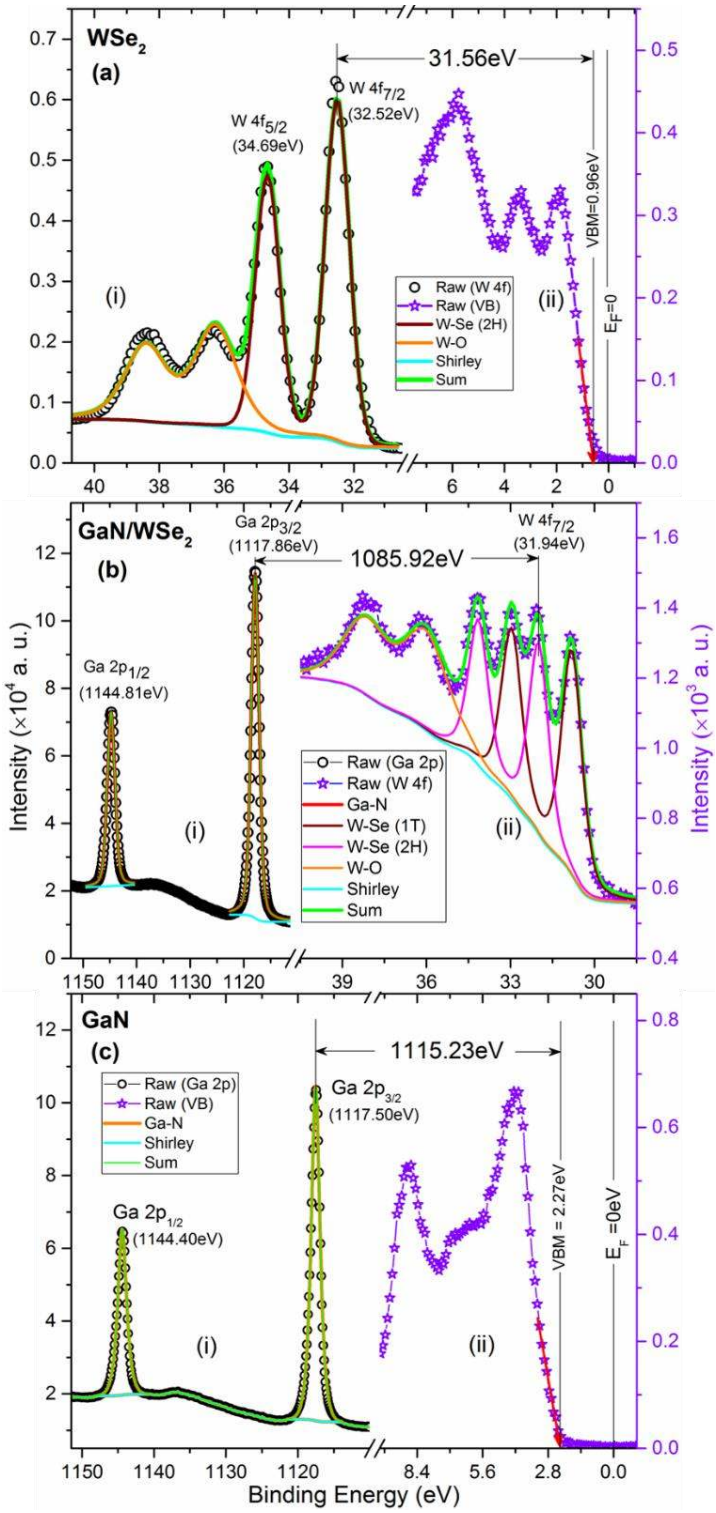

Figure 5a (i and ii) present the W 4f core-level and valence band spectra for SL-WSe_2. b(i and ii) show the spectra of Ga 2p and W 4f core-levels for GaN/SL-WSe_2. c(i and ii) show Ga 2p core-level and valence band spectra acquired on GaN epilayer. The peak positions of core-levels are shown in parentheses.

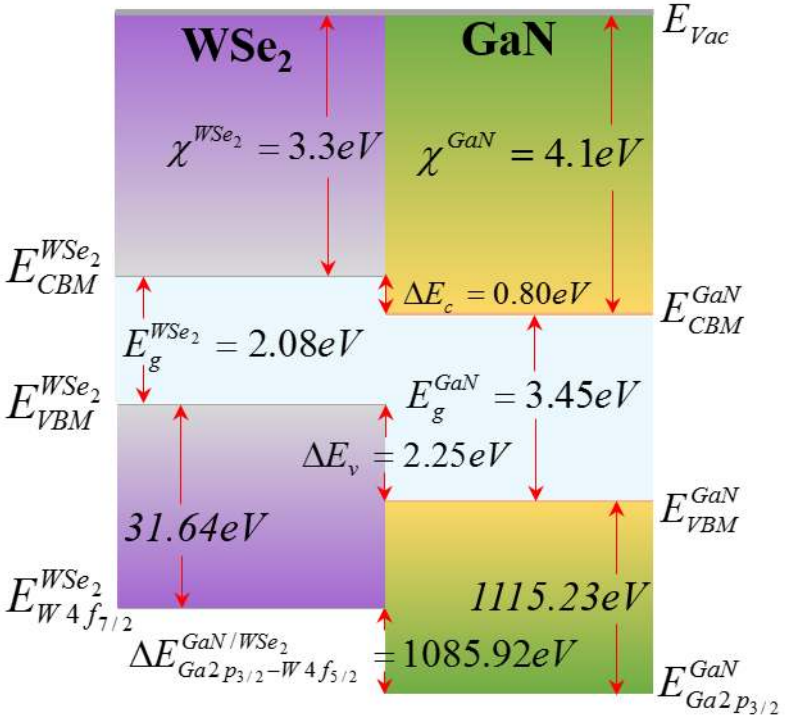

Figure 6 shows the schematic representation of type II band alignment at GaN/SL-WSe_2 heterointerface.

TOC

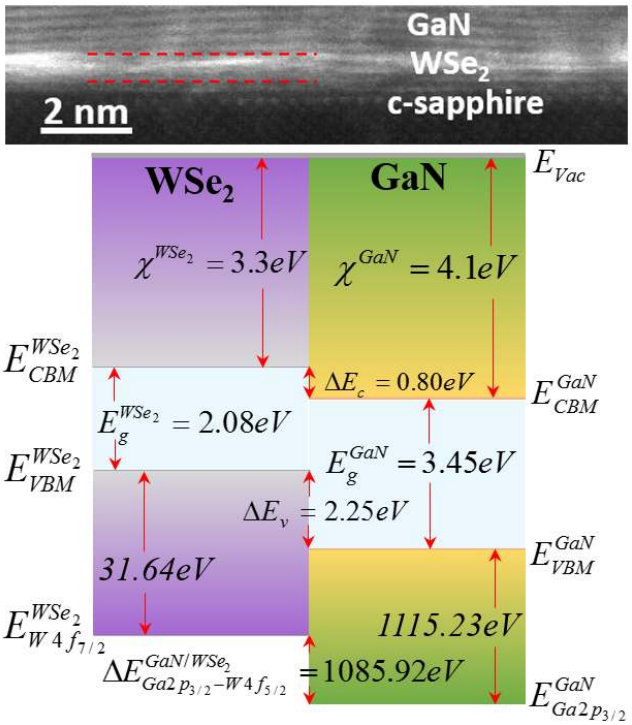
GaN
WSe2
c-sapphire
2 nm
WSe2
GaN
χ^WSe2 = 3.3eV
χ^GaN = 4.1eV
E_Vac
E^WSe2_CBM
ΔE_c = 0.80eV
E^GaN_CBM
E^WSe2_g = 2.08eV
E^GaN_g = 3.45eV
E^WSe2_VBM
ΔE_v = 2.25eV
E^GaN_VBM
31.64eV
1115.23eV
E^WSe2_W4f7/2
ΔE^GaN/WSe2_Ga2p3/2–W4f5/2 = 1085.92eV
E^GaN_Ga2p3/2